Relative intensity noise in a multi-Stokes Brillouin laser

Ananthu Sebastian, Irina Balakireva, Schadrac Fresnel, Stephane Trebaol, Pascal Besnard

Research Article | Vol. 26, No. 26 | 24 Dec 2018 | OPTICS EXPRESS 33700
Optics EXPRESS

Relative intensity noise in a multi-Stokes Brillouin laser

ANANTHU SEBASTIAN, IRINA V. BALAKIREVA, SCHADRAC FRESNEL, STÉPHANE TREBAOL, AND PASCAL BESNARD*

Univ Rennes, CNRS, Institut FOTON - UMR 6082, F-22305 Lannion, France
**pascal.besnard@enssat.fr*

Abstract: We investigate the relative intensity noise (RIN) properties of a multi-Stokes Brillouin fiber ring laser. We experimentally analyse the intensity noise of each Stokes wave and study the noise dynamics of the cascaded Brillouin scattering process. We observe up to 20 dB/Hz intensity noise reduction compared to that of the RIN input pump laser. We examine the impact of the fiber ring quality factor on the laser RIN features such as amplitude reduction and relaxation frequency. We also investigate the influence of the Brillouin gain detuning on the RIN reduction. A numerical model based on a set of coupled-mode equations replicates the experimental observations. Our study enables us to determine the optimal parameter values to operate the multi-Stokes laser in the low noise regime.

Introduction

Stimulated Brillouin Scattering (SBS) process [1] generate considerable interests in laser physics communities for its ability to induce low noise lasers [2, 3]. Linewidth narrowing and intensity noise reduction have been demonstrated in various systems as fiber rings [4], whispering gallery mode microresonators [5] or planar waveguide structures [6] to only name a few. Those systems are made of nonlinear materials as silica [7], chalcogenide [8], silicon nitride [9], crystal fluoride [10] or silicon [11]. SBS low noise lasers are attractive candidates for a large panel of applications ranging from coherent optical communications [12], RF signal generation [13] and processing [14] to sensors [15]. Laser performances have been widely studied and in particular intensity [4, 16] and frequency noises [9, 17] reaching even metrological performances [18, 19]. Cascading the SBS process by using one Stokes order, as a pump, for the next red shifted Stokes wave brings the possibility to produce a comb source with equally spaced lines [20].

A remaining question concerns the potential of cascading the SBS process to improve the intensity and frequency noise reduction. Recently, a theoretical paper predicts that intensity and frequency noise reduction are not possible by cascading the SBS process [21]. It should be noted that noise reduction has been already observed in Brillouin laser when second Stokes order starts to lase [8, 22]. In this paper, we demonstrate that, under a specific operating regime, Stokes line intensity noise can be reduced up to 40 dB/Hz respect to the input pump RIN. Moreover, we report the complex RIN dynamics of a multi-Stokes Brillouin laser (MBL) in various configurations. In particular, we investigate the role of the ring cavity Q-factor on the relaxation of oscillation and on the RIN reduction of the MBL. Our numerical simulations support our experimental observations.

The paper is organized as follows: in Section 1 we describe the experimental setup and the fiber ring resonator used for the present study. In Section 2, we introduce the MBL model based on coupled-mode equations. In Section 3, we derive the stationary response of MBL and recall its working principle. In Section 4, we study the RIN behavior of Stokes lines as a function of the input pump power and determine the conditions to obtain low-intensity noise laser emission. We finally discuss the role of cavity lifetimes and gain detuning on the RIN performance of the MBL.

#348627 https://doi.org/10.1364/OE.26.033700
Journal © 2018 Received 24 Oct 2018; revised 1 Dec 2018; accepted 2 Dec 2018; published 11 Dec 2018

Optics EXPRESS

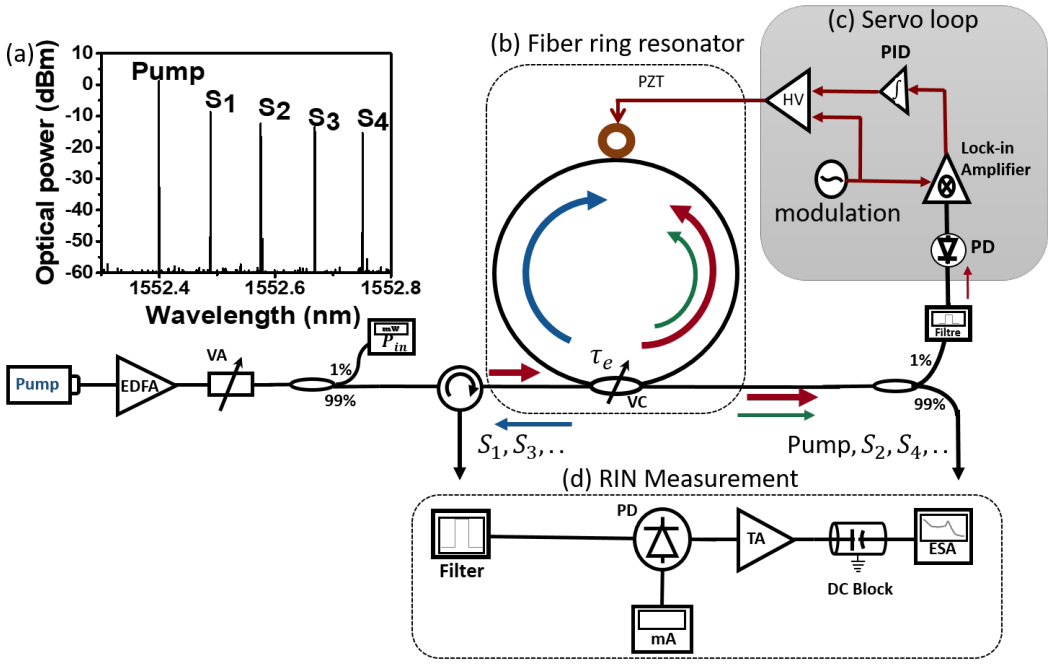

Fig. 1. Experimental setup to study the lasing properties of multi-Stokes Brillouin Laser. Pump: Koheras continous wave laser, EDFA: Erbium-doped fiber amplifer, VA: variable attenuator , VC: Variable coupler, PZT: Piezoelectric transducer, Filter: Yenista optical filter, PD: Photodiode, PID: Proportional-integral differential amplifier, HV: High-voltage amplifer, TA: Transimpedance Amplifier, ESA: Electrical spetrum analyzer. The fiber ring cavity is composed of 20 m polarization maintaining fiber spooled around a PZT. Red line: Pump wave, Blue: Stokes 1 wave , Green: Stokes 2 wave.

1. Experimental Details

1.1. Fiber Ring Cavity

The central element of the MBL is composed of a fiber ring resonator depicted in Fig.1(b). The gain or losses inside the resonator is quantified by the intrinsic cavity lifetime ($\tau_0/2$) and the coupling strength by the coupling lifetime ($\tau_e/2$). The total photon lifetime of the resonator is expressed as $1/\tau = 1/\tau_0 + 1/\tau_e$ bringing to the Q-factor equation $Q = \omega\tau/2$. The resonator is made of a 20 m polarization-maintaining fiber corresponding to a free-spectral range (FSR) of 10 MHz. The light is coupled in and out through a variable coupler allowing to vary the coupling coefficient and then the Q-factor of the resonator [23]. In the present study, we consider two resonator configurations which we call: the high-Q resonator ($Q_h = 6 \times 10^8$) and the low-Q resonator ($Q_l = 2 \times 10^8$). The finesse of the cavity in the high and low-Q configurations is 61.6 and 8.2 respectively. Cavity parameters are extracted using the cavity ring down method [23]. The low-Q factor and high-Q factor cavities are in the overcoupling ($\tau_0 > \tau_e$) and the undercoupling ($\tau_0 < \tau_e$) regimes respectively. In terms of Brillouin laser performances, the overcoupling regime implies a higher output power at the price of higher lasing threshold ($P_{th} = 26.5$ mW) with respect to the undercoupling operation ($P_{th} = 7.2$ mW). As it will be shown later, the Q-factor of the resonator impacts the RIN features of the MBL (Sec. 4.3).

Optics EXPRESS

1.2. Experimental setup

The experimental setup is illustrated in Fig.1. The fiber ring cavity is optically pumped using a continuous wave (CW) 1.7 kHz line-width laser emitting at 1552.4 nm. The laser output power is amplified before the cavity injection. A motorized variable optical attenuator helps to control the input power in the MBL. 1% of the input pump power is collected for power monitoring.

The laser pump signal is introduced in the cavity via a circulator and a coupler, and then propagates clockwise in the cavity (red arrow). The circulating pump wave initiates Brillouin amplification in Stokes 1 wave traveling in the opposite direction (blue arrow). For sufficiently high pump power ($P_{in} = P_{th}$), Brillouin lasing threshold is reached giving rise to efficient Stokes 1 emission outside the resonator. Stokes 1 wave can, in turn, play the role of pump laser for Stokes 2 wave (green arrow), the cascading process is then activated.

Cavity servoing

The laser threshold for the various Stokes waves can be drastically reduced when the pump signal is resonantly coupled in the cavity. This configuration can be achieved by locking a cavity resonance to the CW pump laser. We implement a derivative spectroscopy stabilization method [24], its setup is shown in the gray box in Fig.1(c). The actuator consists in a piezoelectric (PZT) ceramic cylinder wrapped by few meters of fiber. Varying the voltage on the piezoelectric implies a modification of the cavity length and then a control of the frequency position of the cavity resonances.
We apply a fast modulation frequency of 10 kHz and a slow modulation of 5 Hz on the PZT through a high-voltage amplifier. The slow modulation scans the cavity resonances. High-frequency dithering at 10 kHz creates derivative error signal from a lock-in amplifier. Actuator signal is produced by sending the error signal to a PID controller. Using this technique the cavity is maintained in resonance with the pump laser during MBL operation.

RIN measurement

The usual measurement method of intensity noise characterization consists in the acquisition of the Power Spectral Density (PSD) of the intensity noise of a laser line [25]. We will, therefore, use an Electrical Spectrum Analyzer (ESA) to obtain the PSD of the electrical signal at the detection level. The intensity noise measurement bench is schematically described in the Fig. 1(d). The detection system consists of a photodiode with a bandwidth from DC to 1 GHz, a transimpedance amplifier (TA) with a variable bandwidth depending on the gain, but not exceeding 200 MHz, and a "DC-Block" module with very low cut-off frequency (1 Hz), to remove the DC component of the electrical signal in order to avoid damaging of the ESA. In Section 4, we report analysis of the MBL RIN measurements for different Stokes lines.

2. Theoretical model

To study theoretically the RIN of generated Stokes orders in the cascaded SBS process, we extend the model described by W. Loh et al. [26] in the framework of single Stokes generation, to the MBL. The model, based on the coupled modes formalism [27], depicts the temporal dynamics of $2N + 1$ coupled-mode equations, in which N is the maximum number of Stokes waves under

Optics EXPRESS

consideration:

$$\frac{\partial A_0}{\partial t} = -\frac{1}{\tau}A_0 - iq_0\omega_0 A_1\rho_1 + \sqrt{\frac{2}{\tau_e}}Se^{i\sigma_0 t}, \quad (1)$$

$$\frac{\partial A_\eta}{\partial t} = -\frac{1}{\tau_\eta}A_\eta - iq_\eta\omega_\eta\left[A_{\eta-1}\rho_\eta^* + \delta_{\eta\neq N}A_{\eta+1}\rho_{\eta+1}\right], \quad (2)$$

$$\frac{\partial \rho_\eta}{\partial t} = i\frac{\Omega_b^2-\Omega_\eta^2}{2\Omega_\eta}\rho_\eta - \frac{\Gamma_b}{2}\rho_\eta - ip_\eta A_{\eta-1}A_\eta^*. \quad (3)$$

Here A_η, ω_η, and τ_η are the amplitude, frequency and lifetime of the generated Stokes wave noted η (with $\eta \in [1, N]$). Eq. (1) describes the dynamics of the pumped mode A_0, its angular frequency is $\omega_0 = 1.22\times10^{15}$ rad/s. τ_e is the pump-resonator coupling time constant. ρ_η and Ω_η are the amplitude and frequency of the density wave label η. $\Gamma_b = 2\pi\times30\times10^6$ rad/s is the loss rate of the density wave and $\Omega_b = 2\pi\times11.55\times10^9$ rad/s is the acoustic frequency at which the SBS gain is maximum. These two parameters are experimentally extracted. We consider a constant Brillouin Stokes shift over the cascading process, which means, $\Omega_b = \Omega_\eta$ for all η. Coefficients q_η and p_η are:

$$q_\eta = \frac{\gamma_e}{4n_0^2\rho_0}\Lambda_\eta, \quad \text{and} \quad p_\eta = \frac{\epsilon_0\gamma_e n_0^2\Omega_\eta}{4v^2}\Lambda_{\rho_\eta}, \quad (4)$$

where $\gamma_e = 1.5$ is the electrostrictive constant, ϵ_0 is the vacuum permittivity, $n_0 = 1.44$ is the refractive index for silica, $\rho_0 = 2200$ kg/m^3 is the equilibrium density of the material, v is the velocity of the acoustic wave. In the present work, the resonator is composed of fiber. We can reasonably consider that modes are similarly confined in the fiber and then fix the value of mode overlaps [18] Λ_η and Λ_{ρ_η} to 1. The amplitude of the pump wave is $S = \sqrt{P/(V_{ph}\epsilon_0)}$, where P is the power of the laser (in watts) and $V_{ph} = 1.56\times10^{-9}$ m^3 is the optical mode volume of the fiber ring cavity.

The total lifetime τ_η of each Stokes wave can be found by $1/\tau_\eta = 1/\tau_{0\eta} + 1/\tau_{e\eta}$ where $\tau_{0\eta}$ is the intrinsic lifetime (cavity losses) and $\tau_{e\eta}$ is the coupling lifetime. For reasons of simplifications, we consider the lifetimes equal for all waves, and we write $\tau_\eta = \tau$, $\tau_{0\eta} = \tau_0$, $\tau_{e\eta} = \tau_e$, $q_\eta = q$, and $p_\eta = p$. In this article, we study the case of zero detuning between cavity resonance and the laser wavelength, which means $\sigma_0 = \omega_L - \omega_0 = 0$. Experimentally, this configuration is maintained by the cavity servoing. We will see in the following that this resonant pump configuration is a key factor to get good matches with the experimental results.

RIN Simulation

To calculate RIN, we introduce noise in the pump term of Eq. (1) as $S_0 = S + f_r$. Here f_r represents the fluctuations of the pump amplitude approximated by a Langevin white Gaussian noise source with $\langle f_r(t)f_r^*(t')\rangle = C\delta(t-t')$, where C is the auto-correlation strength of f_r. C is used as a fitting parameter and it disappears after the normalization of Stokes RIN to the input pump RIN. Numerical simulations correspond to time streams of 7 ms with a time resolution of 3 ns. The corresponding quite large number of events justify the use of a Gaussian distribution, instead of a Poissonian one through the central limit theorem [28]. Then we take the amplitudes fluctuations $\delta|A_\eta| = |A_\eta| - |A_\eta|_S$, and we find their spectral densities $S^p_{\delta|A_\eta|}$ by converting them in the frequency domain and multiplying by the complex conjugate. RIN is finally determined by [26]:

$$\text{RIN} = \frac{8S^p_{\delta|A_\eta|}}{|A_\eta|_S^2} \quad (5)$$

RIN curves are obtained from the average over 20 computations.

Optics EXPRESS

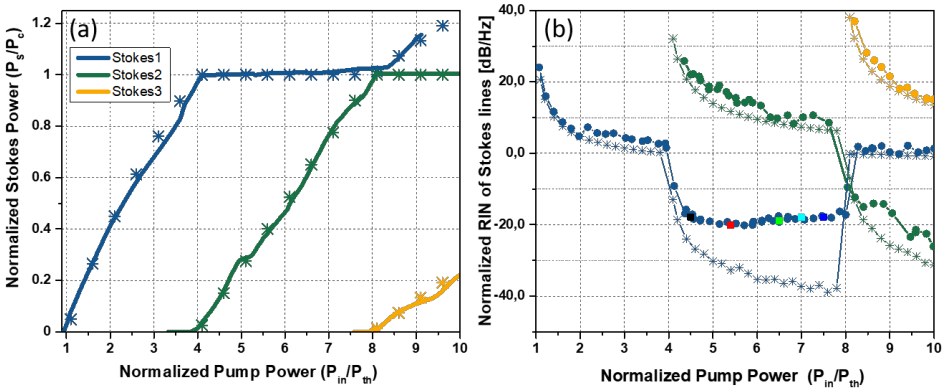

Fig. 2. (a) Output Stokes power (P_s) normalized to the circulating power (P_c) versus input pump power (P_{in}) normalized to the Stokes 1 lasing threshold (P_{th}). (b) RIN of Stokes lines normalized to the input pump RIN. RIN amplitude is measured at 4 kHz from the carrier. Straight lines and full dots are experimental results. Stars are simulation results. Results are obtained with the "low-Q cavity" Brillouin laser, P_{th} = 26.5 mW. Square symbols correspond to numerical simulations including gain detuning (black $\Delta\nu$ = 100 kHz, red $\Delta\nu$ = 250 kHz, green $\Delta\nu$ = 400 kHz, blue light $\Delta\nu$ = 400 kHz, deep blue $\Delta\nu$ = 450 kHz)

3. Cascade effect in Brillouin fiber laser

We study the stationary response of a resonantly pump fiber cavity through the output power Stokes (P_s) as function of the input pump power. We recall the principle of the cascaded generation of Brillouin Stokes waves in such a resonator. We plot in Fig.2(a), the evolution of output Stokes lines 1, 2, and 3 as function of the input pump power for the low-Q factor cavity. Independent Stokes lines output power characterization are performed by optical filtering. Straight lines and stars correspond to experimental results and numerical simulations respectively.

Above the normalized pump power P_{in}/P_{th} = 1, the pump circulating power is clamped. This operating point corresponds to the onset of coherency in the first Stokes order. Indeed, the Brillouin gain, induced by the pump laser, balances the linear losses experience by Stokes 1 line: efficient stimulated Brillouin emission occurs (blue curve). When the power in Stokes 1 (S1) reaches the normalized output power needed to compensate S2 linear losses, coherent emission also takes place; the cascaded process is on. The cascaded generation of multiple Stokes waves has been treated analytically by Toyama et al. [29] considering resonant pumping of the cavity and constant Brillouin gain for the all Stokes orders. Analytical expressions for the Stokes power evolution versus input pump power are derived from Eqs. (1, 2, 3) (see Appendix). The model gives rise to similar results than previously reported models in the literature [21, 29].

It is worth to mention that when the output power of a Stokes order ($\eta+1$) evolves monotonically with the pump power, the output power of the pumping Stokes order (η) is constant due to the clamping effect [30]. Stokes lines output power alternate between monotonous evolution and constant power emission when the clamping effect occurs due to the onset of coherent emission on the $\eta+1$ Stokes wave. This effect is determinant to explain the main contribution of the paper related to the intensity noise reduction of MBL discussed in the next Section.

Optics EXPRESS

4. Relative intensity noise of multi-Stokes laser

This Section reports the main contribution of this paper regarding the intensity noise evolution of a multi-Stokes laser. Since our objective is to determine the Brillouin laser RIN transfer function, we choose to make measurements independent of the RIN behavior of the pump by normalizing our Stokes RIN measurement with respect to the RIN of the input pump. This normalization permits to get rid of the pump-RIN features, as for example intrinsic relaxation frequency, which do not relate to the Brillouin processes themselves. This normalization simplifies the identification of RIN features added through the cascaded processes. Moreover, it allows our experimental observations to be compared to numerical simulations, for which an ideal white frequency noise is considered for the pump RIN. In Section 4.1, we scrutinize the overall evolution of the RIN for the Stokes waves $S1$, $S2$, and $S3$ as function of the input pump power. Then, in Section 4.2, we focus on the RIN behavior for individual Stokes lines $S1$ and $S2$. In Section 4.3, we discuss the impact of the cavity Q-factor on the MBL RIN. In Section 4.4, the impact of gain detuning is evaluated. All experimental RIN results are compared to numerical simulations performed with experimentally extracted parameters.

4.1. RIN versus the cascade process

As a first step in the study of RIN in MBL, we discuss the behavior of the RIN at 4 kHz from the carrier. We report in Fig.2(b) the RIN behavior of the three first individual Stokes lines as function of the input pump power. Dotted lines correspond to experimental RIN measurements and starred lines to numerical simulations. We first focus on the $S1$ RIN. For a normalized input pump power of 1, corresponding to the $S1$ threshold, $S1$ RIN highlights 20 dB/Hz excess RIN with respect to that of normalized input pump. As mentionned before, the pump clamping between $1\times P_{\text{th}}$ and $4\times P_{\text{th}}$, implies a transfer of pump fluctuations towards $S1$ [17]. Those fluctuations are amplified through the Brillouin gain explaining the excess noise. While going away from the $S1$ threshold, the $S1$ output power increases implying a progressive decrease of the RIN towards the input pump RIN level. A tiny increase of the Stokes 1 RIN between $2\times P_{\text{th}}$ and $4\times P_{\text{th}}$ can be observed on Fig.2(b). We attribute this kink to the contribution of a side longitudinal cavity mode that induces intensity fluctuations on the main longitudinal mode. It is worth to notice that, in single mode Brillouin laser, the output Stokes RIN can even be lower than the input pump RIN. The noise reduction is strongly dependent of the cavity and Brillouin gain coefficients [16], and the laser sensitivity to environmental perturbations as in a usual laser. In the present work, we take advantage of the SBS cascade effect to reduce Stokes noise level below the input pump RIN as described below.

Above $4\times P_{\text{th}}$, which corresponds to the $S2$ lasing threshold, the $S1$ experiences an abrupt RIN reduction up to 20 dB compared to the input pump RIN level. This reduction originates from the clamping effect of $S1$ due to the appearance of the stimulated $S2$ emission. In that regime, the "gain=losses" condition acts as a driving force to maintain the $S1$ output power constant [See Eq. (7)]. Thereby, any intensity fluctuations of $S1$ are attenuated. At $8\times P_{\text{th}}$, coherent $S3$ emission arises. $S2$ becomes an efficient pump for $S3$, and similarly, intensity noise reduction occurs for $S2$ above the $S3$ lasing threshold power. Since $S2$ output power is clamped, $S1$ output power increases again proportionally to the input pump power. The consequences on the $S1$ RIN are instantaneous and manifest as an increase of noise level toward the input pump one. Concerning the $S3$ RIN, close to the threshold, its RIN reaches 36 dB/Hz in excess to the pump laser RIN and progressively shortens towards the input pump RIN level. This high RIN level can be attributed to the noise transfer through the cascade effect. Indeed, SBS process implies energy conservation between involved waves. Then, RIN of uphill waves are transfered, and even amplified, to downhill waves. Moreover, as mention by Behunin et al. [21] spontaneous anti-Stokes emission can also degrade RIN of Stokes waves (that is not taken into account in our model).

Optics EXPRESS

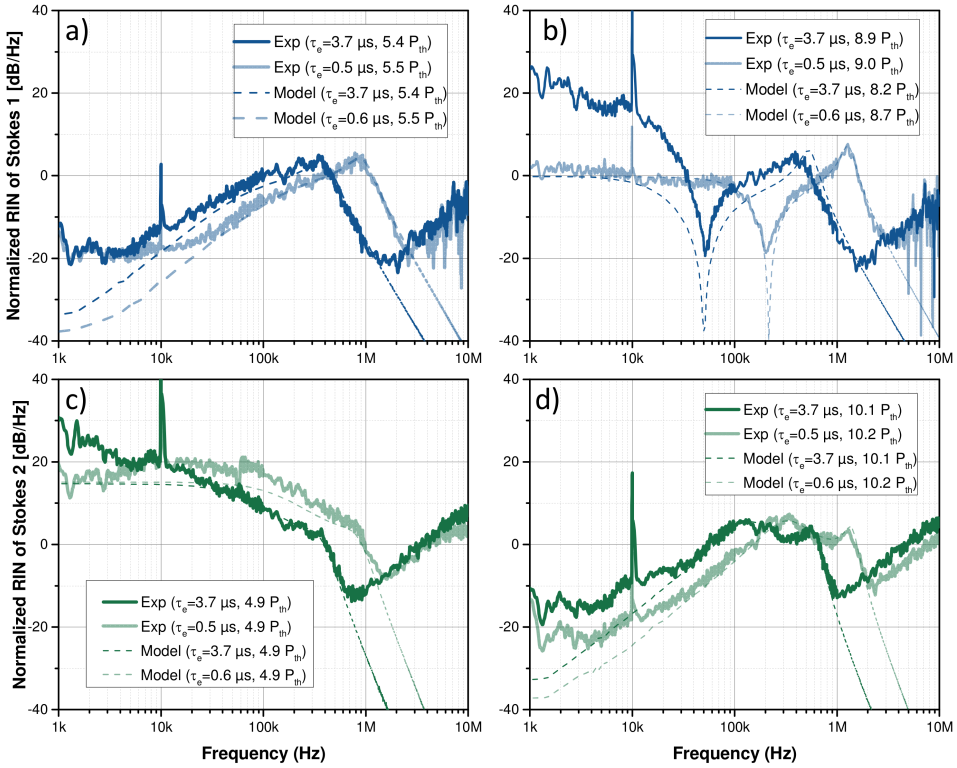

Fig. 3. Normalized RIN of Stokes 1 (a, b) and Stokes 2 (c, d) lines for various input pump powers. Full and dashed lines hold for experimental and simulation results respectively. Deep and light colors refered to high (τ_0 = 1.4 μs, τ_e = 3.7 μs) and low-Q factors (τ_0 = 1.4 μs, τ_e = 0.5 μs) respectively. The peak observed at 10 kHz originates from the high-frequency modulation of the servoing scheme

Simulation procedure has been described in section 2. RIN behavior is very well reproduced by the numerical simulations (starred lines) in particular: (i) the monotonous reduction of RIN in free running regime and (ii) the sudden reduction in the clamping regime. A discrepancy in the RIN reduction amplitude between the model and the experiment exists in the clamping regime. The model expects up to -40 dB/Hz reduction when the experimental results tend to -20 dB/Hz. This point will be addressed in section 4.4.

In this Subsection, we have shown the substantial impact of the clamping effect on the intensity noise properties of the laser. In other words, once the Stokes line labeled $\eta + 1$ reaches the lasing threshold power, the "gain=loss" condition implies the clamping of the Stokes wave η playing the role of the pump. In this regime, fluctuations of Stokes η are sharply reduced, and up to 20 dB/Hz reduction compared to the RIN of the input pump laser is experimentally observed. Similar noise fluctuations reduction have been demonstrated in semiconductor optical amplifier (SOA) used in the saturation regime [31, 32].

In the following Subsection, we describe in detail the RIN behavior of individual Stokes order for various operating points to show the rich dynamics of RIN when MBL emission takes place.

Optics EXPRESS

4.2. RIN of individual Stokes lines

To get more insight on the intensity noise of individual Stokes lines, we propose to study the complete RIN noise behavior for various input pump powers.

We plot in Fig.3 the RIN of $S1$ (blue color) and $S2$ (green color) between 1 kHz and 10 MHz in two operating points: i) in clamping regime [Fig.3 a) and d)] ii) in monotonous regime [Fig.3(b) and (c)]. We will first focus on light blue curves corresponding to the low Q-factor cavity.

In the clamping regime [Fig.3(a) and (d)], a 20 dB reduction of the $S1$ and $S2$ RIN occurs at low offset frequency (< 100 kHz). As explained previously, the onset of laser emission on $S_{\eta+1}$ implies the clamping of S_η power and then the attenuation of its RIN amplitude. By analogy to a class B laser, where coupling between photons and electrons take places, the RIN of the Brillouin laser in single Stokes operation ($P_{\text{in}} < 4 \times P_{\text{th}}$)) features a relaxation frequency resulting from the coupling between photons and phonons [26]. An analytical expression for the relaxation frequency in single Stokes regime (P_{in} from 1 to 4 $\times P_{\text{th}}$) can be expressed as [26]

$$f_{\text{R}} = \frac{1}{2\pi}\sqrt{\frac{|A_1|^2}{|A_0|^2} * \frac{2\Gamma_b}{\tau^2}\left(\frac{2}{\tau} + \frac{\Gamma_b}{2}\right)^{-1}} \tag{6}$$

Figure 4 yields extracted frequency of relaxation from Stokes 1 in both cavity configurations (symbols). The results of calculations of Eq. (6) are plotted in lines. The frequency of relaxation evolves proportionally to the square root of the pump term like a class B diode laser [33]. Both cavities show an excellent superposition between the analytical expressions and experimental results.

For $P_{\text{in}} > 4 \times P_{\text{th}}$, the laser shifts from single to multi-Stokes Brillouin lasing and then the class B analogy is not anymore valid. The onset of $S3$ line for $P_{\text{in}} > 8 \times P_{\text{th}}$ implies the appearance of multiple frequencies of relaxation originating from the complex Stokes waves coupling [21] as shown on the RIN of Stokes 2 [Fig.3(d), inside the interval (100 kHz, 2 MHz)].

In the monotonous regime [Fig.3(b) and (c)], when the considered Stokes order has an output power that increases monotonically with the input pump power, RIN amplitudes at low offset frequency rise to at least the input pump RIN level. In this regime the noise transfer channel from "pump" to Stokes line is open. It corresponds to noise transfer from input pump toward $S1$ in Fig.3(b) or from $S1$ toward $S2$ in Fig.3(c).

As shown in Fig.3, our experimental observations are well reproduced by numerical simulations based on the model exposed in Section 2. In particular noise reduction at low offset frequencies, complex relaxation frequency shape and position and noise amplitude are well reproduced. As expected, the model shows that the cavity lifetime and the pump power determine the frequency of relaxation resonances.

Similar RIN behavior is observed experimentally for incoming Stokes orders alternating sequences of low RIN level at low frequency offset when the Stokes line is clamped and high RIN level when the noise of previous Stokes order is efficiently coupled through SBS process.

4.3. Impact of photon lifetimes

In this Section, we highlight the fundamental role of the cavity parameters on the RIN properties of the MBL. For this purpose, we vary the coupling coefficients to modify the coupling lifetime τ_e from 0.5 μs to 3.7 μs. The intrinsic lifetime, τ_0 of the resonator remains the same since no additional losses are introduced (τ_0 = 1.4 μs). Details about the two configurations and their characterizations are given in Section 1.1.

Figure 3 reports the RIN behavior for two cavity configurations. The light and deep colored curves refer to the low-Q (shorter photon lifetime) and high-Q (longer photon lifetime) resonator configuration respectively. By comparing the RIN of both configurations, two main features can be associated with the total photon lifetime values.

Optics EXPRESS

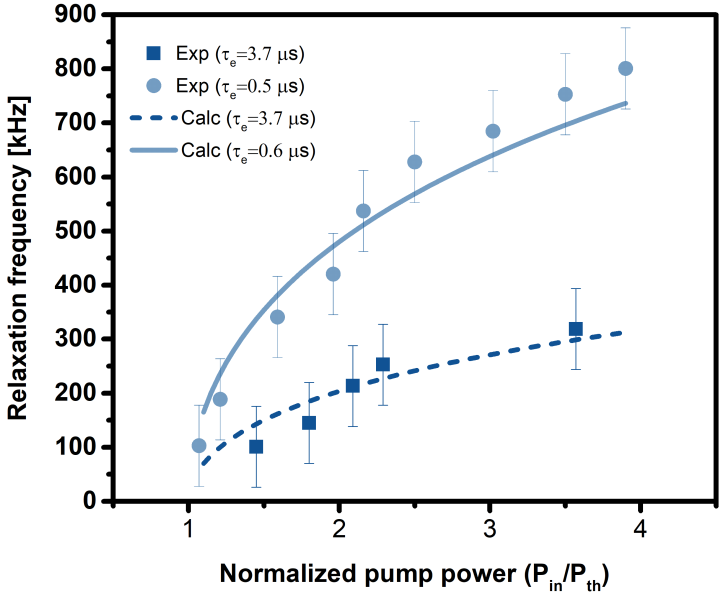

Fig. 4. Relaxation frequency as function of the normalized pump power for low-Q (light blue) and high-Q (deep blue) cavities. Lines represent the results of calculation of Eq. (6). Error bars (±75 kHz) represent the average possible misreading of relaxation frequency on RIN curves.

First, the frequency of the relaxation resonance is directly determined by the phonon lifetime and the total photon lifetime of the cavity as shown by Eq. (6). Indeed, the shorter lifetime cavity (low-Q) systematically highlights a larger relaxation frequencies for $S1$ and $S2$ lines. This behavior has been reported in Fig.4, showing the frequency redshift versus input pump power (1 and 4 $\times P_{\text{th}}$) for both configurations.

Secondly, low offset frequency Stokes RIN levels are systematically higher for the high-Q resonator. As an example, the $S1$ RIN in the high-Q configuration (deep blue) presents an excess noise of 25 dB/Hz with respect to the low-Q configuration (light blue) [Fig.3(b)]. A possible explanation can be found in the relative frequency fluctuations between the input pump laser and the cavity resonance. The steeper the cavity resonance is, the better the frequency fluctuations are transformed into intensity fluctuations. Then, the high-Q resonator RIN is more sensitive to thermal [18] and mechanical noise [16] and favor the transfer of low frequency pump fluctuations. Those effects are not taken into account in the present model, which may explain the discrepancy in the RIN level observed at low offset frequency in Fig.3.

4.4. *Impact of gain detuning*

In the numerical simulations presented in previous sections, we consider a zero-detuning operation of the $S1$ wave, which corresponds to a match between the frequency of the density wave Ω and the frequency of the maximum of the gain Ω_b. This configuration is very difficult to obtain since it implies that the SBS shift corresponds to a multiple integer of the cavity FSR. In general, this condition is not fulfilled, even if a judicious choice of the pump wavelength helps to reach it, as the Brillouin shift (Ω_b) is dependent on the pump wavelength by $\Omega_b = 4\pi n_{\text{eff}} V_A/\lambda_p$ with n_{eff}, λ_p the effective index and the pump wavelength respectively.

To evaluate the impact of a gain detuning, we include in numerical simulations the gain detuning $\Delta\nu = (\Omega_b - \Omega)/2\pi$. This detuning implies that SBS Stokes waves are resonant at a

Optics EXPRESS

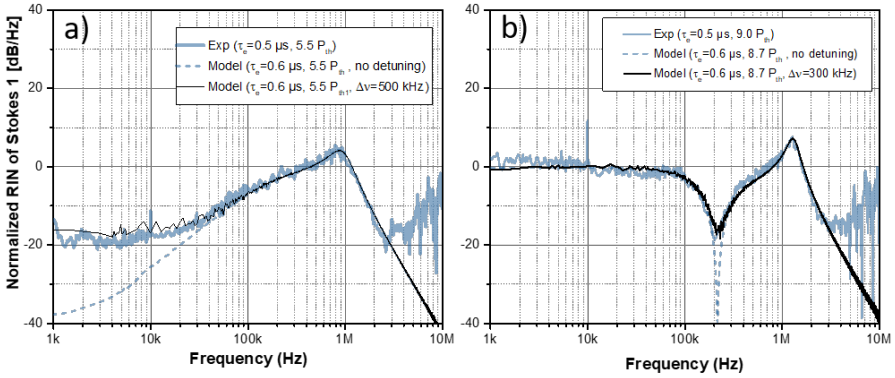

Fig. 5. Evolution of the Stokes 1 RIN in function of the gain detuning for a pump power of a) 5.5 P_{th} and b) 9 Pth in the low-Q cavity configuration

frequency, which does not correspond to the frequency of the maximum Brillouin gain.

Figure 5 focuses on the impact of the gain detuning on the RIN features of the Stokes 1 in (a) the clamped regime and (b) free running regime for the "low-Q cavity" configuration. Including the gain detuning allows one to fit much better the experimental Stokes 1 RIN. Indeed, on Fig.5(a), we fit the Stokes 1 RIN by including a gain detuning of 500 kHz in the numerical simulations. This RIN at low frequency is much better reproduced suggesting that, even a weak detuning (500 kHz) with respect to the gain linewidth (30 MHz), strongly impacts the RIN-reduction performances of the Stokes 1 by 20 dB at 1 kHz. Similarly, at $9 \times P_{\text{th}}$, by including a gain detuning of $\Delta\nu = 300$ kHz in the numerical simulations of the Stokes 1 RIN, the sharp deep profile observed around 200 kHz is attenuated and tends to that of the measurements. To conclude this preliminary study on the impact of detuning in a MBL, we plot on Fig.2(b), numerical evaluation of the Stokes 1 RIN level at 4 kHz from the offset frequency (squared symbols). Experimental data are fitted by adjusting the gain detuning parameter (details in the caption of Fig.2). The discrepancy between experiment and simulations in the pump range $4 \times P_{\text{th}}$ to $8 \times P_{\text{th}}$ have to be attributed to the slight gain detuning that strongly limits the overall RIN-reduction performances of the MBL by up to 20 dB in the present study. These results suggest that further investigations have to be done to design optimized cavity that satisfy zero detuning conditions.

Conclusion

In this paper, we demonstrate that low offset frequency RIN of considered Stokes lines can be strongly attenuated when operating in the clamping regime. This is particularly true for first Stokes orders where 20 dB/Hz RIN reduction is observed compared to the input pump RIN. Our study shows that up to 40 dB/Hz RIN reduction is reachable if zero-detuning regime is achieved. When operating in single Stokes regime, our study of the impact of photon lifetime on the relaxation frequency shows an analogy between Brillouin Fiber laser and Class B laser behavior. Experimental observations are well supported by numerical simulations that reproduced the main features of multi-Stokes RIN. Our study gives inputs to design optimized Brillouin fiber laser in term of RIN reduction. Our results suggest driving the Brillouin laser between 5 to 7 times the Stokes 1 threshold power. The fact that our results obtained in fiber ring resonators are normalized in terms of threshold power and input pump noise allows the transposition of our observations to other photonic structures as planar micro-cavity whatever the type of materials is used.

Optics EXPRESS

Appendix A: Stationary response

The stationary response can be found by setting all derivatives in Eqs. (2) and (3) to zero and by checking the joint solutions of the equations. The solutions can be found for any N using three equations. Two of them do not depend on the parity of N:

$$|A_{N-1}|^2 = \frac{K_N}{\omega_N}, \tag{7}$$

$$|A_{\eta+2}|^2 = |A_\eta|^2 - \frac{K_{\eta+1}}{\omega_{\eta+1}}. \tag{8}$$

Another one is changing in dependence on the parity of maximum Stokes order N:

$$|A_0|^2 = \frac{2\tau^2}{\tau_e}|S|^2 \times \left[K^{-1}\omega_0|A_1|^2 + 1\right]^{-2}, \text{ if } N = 2, 4, 6... \tag{9}$$

$$|A_1|^2 = \left[\frac{\tau}{\sqrt{\tau_e/2}}\frac{|S|}{|A_0|} - 1\right]\frac{K}{\omega_0}, \qquad \text{if } N = 1, 3, 5... \tag{10}$$

Here $K_\eta = \Gamma_b/(2\tau p_\eta q)$. The technique of the calculations is the following. First, we calculate $|A_{N-1}|^2$ using Eq. (7), and after using Eq. (8) we find $|A_{N-3}|^2$, $|A_{N-5}|^2$ etc. until A_0 if N is odd or A_1 if N is even. After we use Eqs. (9) or (10) and finish the missing lines by Eq. (8) until $|A_N|^2$.

Funding

The present work is supported under project FUI AAP20 SOLBO, with the help of BPI FRANCE and Pôle Images & Réseaux. We thank also UBL for its financial support.

Acknowledgments

The authors would like to thank Sophie Larochelle, Mohamed Omar Sahni and Rodolphe Collin for fruitfull discussions and Frédéric Ginovart for his careful reading of the manuscript.

References

1. E. Ippen and R. Stolen, "Stimulated Brillouin scattering in optical fibers," Appl. Phys. Lett. **21**, 539–541 (1972).
2. S. Smith, F. Zarinetchi, and S. Ezekiel, "Narrow-linewidth stimulated Brillouin fiber laser and applications," Opt. letters **16**, 393–395 (1991).
3. A. Debut, S. Randoux, and J. Zemmouri, "Linewidth narrowing in Brillouin lasers: Theoretical analysis," Phys. Rev. A **62**, 023803 (2000).
4. J. Geng, S. Staines, Z. Wang, J. Zong, M. Blake, and S. Jiang, "Highly stable low-noise Brillouin fiber laser with ultranarrow spectral linewidth," IEEE Photonics Technol. Lett. **18**, 1813–1815 (2006).
5. G. Lin, S. Diallo, K. Saleh, R. Martinenghi, J.-C. Beugnot, T. Sylvestre, and Y. K. Chembo, "Cascaded Brillouin lasing in monolithic barium fluoride whispering gallery mode resonators," Appl. Phys. Lett. **105**, 231103 (2014).
6. T. F. Büttner, M. Merklein, I. V. Kabakova, D. D. Hudson, D.-Y. Choi, B. Luther-Davies, S. J. Madden, and B. J. Eggleton, "Phase-locked, chip-based, cascaded stimulated Brillouin scattering," Optica **1**, 311–314 (2014).
7. S. Molin, G. Baili, M. Alouini, D. Dolfi, and J.-P. Huignard, "Experimental investigation of relative intensity noise in Brillouin fiber ring lasers for microwave photonics applications," Opt. letters **33**, 1681–1683 (2008).
8. K. H. Tow, Y. Léguillon, S. Fresnel, P. Besnard, L. Brilland, D. Méchin, D. Trégoat, J. Troles, and P. Toupin, "Linewidth-narrowing and intensity noise reduction of the 2nd order Stokes component of a low threshold Brillouin laser made of $Ge_{10}As_{22}Se_{68}$ chalcogenide fiber," Opt. Express **20**, B104–B109 (2012).
9. S. Gundavarapu, R. Behunin, G. M. Brodnik, D. Bose, T. Huffman, P. T. Rakich, and D. J. Blumenthal, "Sub-Hz Linewidth Photonic-Integrated Brillouin Laser," arXiv preprint arXiv:1802.10020 (2018).
10. I. S. Grudinin, A. B. Matsko, and L. Maleki, "Brillouin lasing with a CaF_2 whispering gallery mode resonator," Phys. Rev. Lett. **102**, 043902 (2009).
11. H. Shin, W. Qiu, R. Jarecki, J. A. Cox, R. H. Olsson III, A. Starbuck, Z. Wang, and P. T. Rakich, "Tailorable stimulated Brillouin scattering in nanoscale silicon waveguides," Nat. Commun. **4**, 1944 (2013).

Optics EXPRESS

12. A. Choudhary, M. Pelusi, D. Marpaung, T. Inoue, K. Vu, P. Ma, D.-Y. Choi, S. Madden, S. Namiki, and B. J. Eggleton, "On-chip Brillouin purification for frequency comb-based coherent optical communications," Opt. Lett. **42**, 5074–5077 (2017).
13. J. Li, H. Lee, and K. J. Vahala, "Microwave synthesizer using an on-chip Brillouin oscillator," Nat. communications **4**, 2097 (2013).
14. Y. Liu, A. Choudhary, D. Marpaung, and B. J. Eggleton, "Chip-Based Brillouin Processing for Phase Control of RF Signals," IEEE J. Quantum Electron. **54**, 1–13 (2018).
15. F. Zarinetchi, S. Smith, and S. Ezekiel, "Stimulated Brillouin fiber-optic laser gyroscope," Opt. letters **16**, 229–231 (1991).
16. L. Stepien, S. Randoux, and J. Zemmouri, "Intensity noise in Brillouin fiber ring lasers," JOSA B **19**, 1055–1066 (2002).
17. W. Loh, J. Becker, D. C. Cole, A. Coillet, F. N. Baynes, S. B. Papp, and S. A. Diddams, "A microrod-resonator Brillouin laser with 240 Hz absolute linewidth," New J. Phys. **18**, 045001 (2016).
18. W. Loh, A. A. Green, F. N. Baynes, D. C. Cole, F. J. Quinlan, H. Lee, K. J. Vahala, S. B. Papp, and S. A. Diddams, "Dual-microcavity narrow-linewidth Brillouin laser," Optica **2**, 225–232 (2015).
19. M.-G. Suh, Q.-F. Yang, and K. J. Vahala, "Phonon-Limited-Linewidth of Brillouin Lasers at Cryogenic Temperatures," Phys. review letters **119**, 143901 (2017).
20. D. Lim, H. Lee, K. Kim, S. Kang, J. Ahn, and M.-Y. Jeon, "Generation of multiorder Stokes and anti-Stokes lines in a Brillouin erbium-fiber laser with a Sagnac loop mirror," Opt. letters **23**, 1671–1673 (1998).
21. R. O. Behunin, N. T. Otterstrom, P. T. Rakich, S. Gundavarapu, and D. J. Blumenthal, "Fundamental noise dynamics in cascaded-order Brillouin lasers," Phys. Rev. A **98**, 023832 (2018).
22. M. L. Dennis, P. T. Callahan, and M. C. Gross, "Suppression of relative intensity noise in a Brillouin fiber laser by operation above second-order threshold," in *Photonics Society, 2010 23rd Annual Meeting of the IEEE,* (IEEE, 2010), pp. 28–29.
23. Y. Dumeige, S. Trebaol, L. Ghişa, T. K. N. Nguyen, H. Tavernier, and P. Féron, "Determination of coupling regime of high-Q resonators and optical gain of highly selective amplifiers," JOSA B **25**, 2073–2080 (2008).
24. M. Weel and A. Kumarakrishnan, "Laser-frequency stabilization using a lock-in amplifier," Can. journal physics **80**, 1449–1458 (2002).
25. M. Cox, N. Copner, and B. Williams, "High sensitivity precision relative intensity noise calibration standard using low noise reference laser source," IEE Proceedings-Science, Meas. Technol. **145**, 163–165 (1998).
26. W. Loh, S. B. Papp, and S. A. Diddams, "Noise and dynamics of stimulated-Brillouin-scattering microresonator lasers," Phys. Rev. A **91**, 053843 (2015).
27. H. Haus, *Waves and Fields in Optoelectronics* (Prentice-Hall, 1984).
28. K. Petermann, *Laser Diode Modulation and Noise* (Kluwer Academic Publishers, 1988).
29. K. Toyama, S. Huang, P.-A. Nicati, B. Y. Kim, and H. J. Shaw, "Generation of multiple Stokes waves in a Brillouin fiber ring laser," in *Optical Fiber Sensors Conference, pp. 11-14* (1993).
30. S. Ananthu, S. Fresnel, S. Trebaol, F. Ginovart, and P. Besnard, "Improvement of noise reduction in fiber Brillouin lasers due to multi-Stokes operation," in *Conference: Fiber Lasers and Glass Photonics: Materials through Applications,* vol. 10683 (2018).
31. K. Sato and H. Toba, "Reduction of mode partition noise by using semiconductor optical amplifiers," IEEE J. Sel. Top. Quantum Electron. **7**, 328–333 (2001).
32. G. Danion, F. Bondu, G. Loas, and M. Alouini, "GHz bandwidth noise eater hybrid optical amplifier: design guidelines," Opt. letters **39**, 4239–4242 (2014).
33. G. P. Agrawal and N. K. Dutta, *Semiconductor Lasers* (Springer Science & Business Media, 2013).